IEEE Access
Multidisciplinary ⋮ Rapid Review ⋮ Open Access Journal

Received March 4, 2021, accepted March 25, 2021, date of publication April 5, 2021, date of current version April 19, 2021.

Digital Object Identifier 10.1109/ACCESS.2021.3071147

Human Gait Estimation Using Multiple 2D LiDARs

HUU TOAN DUONG AND YOUNG SOO SUH, (Member, IEEE)
Department of Electrical, Electronic and Computer Engineering, University of Ulsan, Ulsan 680-749, South Korea
Corresponding author: Young Soo Suh (yssuh@ulsan.ac.kr)

This work was supported by the 2020 Research Fund of University of Ulsan.

ABSTRACT This paper proposes a human gait estimation algorithm using a multiple 360 degree 2D LiDARs system. The system is fixed on the ground at the shin height to scan human legs during gait. The multiple LiDARs system is to overcome the drawbacks of a single LiDAR system, which could lose data due to occlusion between legs during walking and has a short tracking range. The performance of a sensor fusion system strongly depends on the calibration. In this paper, we propose a calibration method using a cylinder with known radius as a specific marker. In contrast to other methods, the calibration parameters and the cylinder center points at different positions are estimated by a proposed iterative algorithm. The measurement noises in the LiDAR output are considered to increase the accuracy of calibration and human leg center points estimation. Instead of using least square fitting of circle algorithm to estimate the leg center point, a new iterative algorithm which includes measurement noises is proposed. Although multiple LiDARs are used, the discontinuities of leg center points could still happen. Therefore, a quadratic optimization based eighth-order splines algorithm is derived to interpolate and smooth the data. Two configurations of three LiDARs are tested in the experiment. The former is the triangle configuration in which the whole walking path is covered by all three LiDARs. This configuration minimizes the occlusion between legs. The maximum RMSE of step length estimation of this configuration compared with the optical camera system is 0.03m. The latter is the line configuration in which each LiDAR covers a certain walking path sequentially. This configuration maximizes the tracking range. The experiment with 20m straight walking has the RMSE of about 0.10m.

INDEX TERMS Human gait estimation, multiple 2D LiDARs, multiple LiDARs calibration, splines algorithm.

I. INTRODUCTION

The human gait estimation is helpful in various applications and has received extensive attention for decades. It can be used for human identification [1], [2], clinical diagnosis [3], human-robot interaction [4], [5], sport [6] and human navigation [7]. To estimate the human gait, various techniques are presented. They can be divided into two groups: body-attachment and non-body-attachment. In body-attachment group, the Vicon optical camera system [8] which captures the infrared markers attached on the body is a golden system with high precision. Another method estimates the body movement by using inertial measurement units (IMU) attached on different parts of body (foot, waist or wrist) [9], [10]. In the non-body-attachment technique, a camera system without markers can capture and estimate human gait using digital image processing methods [11], [12]. Light detection and ranging (LiDAR) sensor which is another type of optic sensors can also be used [13]. GAITRite system based on floor force plate sensors is known as a gold standard of this group [14]. Although the golden standard methods provide highly accurate gait parameters, they require high operating cost and complicated installation efforts. Body-worn wearable sensor system is light weight and low-cost. However, a major issue of the IMU-based human gait estimation is the accumulation error, which can significantly affect the position estimation.

A 2D LiDAR, which has some advantages of no external markers and simple installation, has been used in autonomous vehicles [15], [16], mobile robot navigation [17], [18] and human gait tracking [19]–[24]. Comparing to a 3D LiDAR, a 2D LiDAR is less expensive both in terms of price and computational cost. The LiDAR can be placed on a moving platform such as mobile robots or smart walkers to track human gait during walking [19], [20]. Some additional sensors such as IMU and encoders need to be installed in these systems to

The associate editor coordinating the review of this manuscript and approving it for publication was John Xun Yang.

estimate the orientation of moving platform. Although these systems can be used in a large space, they are complicated and expensive.

In [21]–[23] and our previous research [24], a 360 degree 2D LiDAR is placed on the ground to track the human shin during walking. The system requires only a single LiDAR so that it is simple to install everywhere in a minute. However, a single LiDAR system has disadvantage of limited tracking range. Because of the small human leg radius and the coarse angular resolution of low cost LiDAR, the human leg tracking range is only few meters. In this paper, we propose a human gait tracking method using a multiple 2D LiDARs system. These LiDARs are placed at the same height on the ground to scan the human legs during walking.

The use of multiple LiDARs gives an issue of calibration to find the relative information between them; thus, many efforts have been made to accurately calibrate the system. Different from multiple 3D LiDARs system that can find the corresponding points of scan data in 3D spaces and directly determine the extrinsic calibration parameters, the multiple 2D LiDARs system is more difficult. One of the most popular methods uses additional sensor such as camera [25], [26] or odometer [27] as a bridge. Schenk *et al.* [28] calibrate the stationary network of multiple 2D LiDARs by matching the trajectories of moving people. Although it does not require additional sensor or external marker, the accuracy is affected by the errors of human trajectory estimation and the placement of LiDARs (they have to scan in a common plane). Another method is to calibrate the multiple LiDARs system on mobile robot by using some specific markers such as orthogonal planes [29], a trihedron [30] or cuboid-shaped corridor [31]. The straight line is fitted to the scan data on the marker plane for each LiDAR, then the intersecting points are used to estimate the calibration parameters. Therefore, these systems require the LiDARs to be placed in different planes and usually are used in mobile robots.

In the proposed method, we use a cylinder to calibrate the multiple 2D LiDARs system. In the calibration process, the cylinder is placed at different positions to capture the scan data. Unlike other methods, our proposed calibration method can estimate the cylinder center points at each position and the calibration parameters. Also, the LiDAR measurement noises, which were neglected in almost previous studies, are considered in this method. We investigate a linear model of measurement errors and the scanning distance of the LiDAR system, then it is used to reduce the error in the calibration process and the human leg tracking algorithm. The human leg is modeled as a circle with a known radius as in [24]; however, a new iterative algorithm is proposed to estimate the leg center point from the LiDAR scan data with the including of measurement errors. After that, a quadratic-optimization based eighth-order splines algorithm is derived to estimate the human legs trajectories by combining legs center points data.

II. SYSTEM OVERVIEW

The proposed tracking system consists of three 2D LiDARs placed on the ground at the same height of 0.3m to track the human leg. Each LiDAR has the sampling rate of 10Hz. As shown in Fig. 1, the system consists of four modules: single LiDAR processing, calibration, data combination and quadratic optimization based splines algorithm.

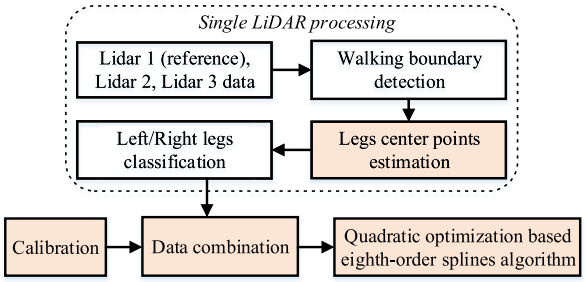

FIGURE 1. Block diagram of the proposed method.

The single LiDAR processing module is applied to each LiDAR data separately. This part is similar to our previous single LiDAR study [24] except the human leg center point estimation part. In contrast with previous study, the measurement errors of LiDAR are explicitly considered in this study and a new center point estimation algorithm is proposed. This part outputs the human legs center points, their estimation error covariances and time stamps of left and right side. The calibration module is to estimate the relative information between the reference LiDAR and the others. The data combination module is to transform the center points data from each LiDAR system into the reference system coordinate using the calibration parameters. Finally, the quadratic optimization based eighth-order splines algorithm outputs the left and right legs trajectories.

III. HUMAN GAIT ESTIMATION

In this paper, a_e denotes the error between the estimated value $\hat{a}$ and the true value $\tilde{a}$, i.e., $\tilde{a} = \hat{a} + a_e$.

A. 2D LiDAR MEASUREMENT MODEL

A sample data s of the 2D LiDAR consists of (d, ϕ, t_s), where d is the distance from the LiDAR rotating core to the object, ϕ is the heading angle and t_s is the sample time stamp (see Fig. 2). This polar coordinate data can be transformed to Cartesian coordinate data (x_s, y_s) as follows: $x_s = d\sin\phi$, $y_s = d\cos\phi$.

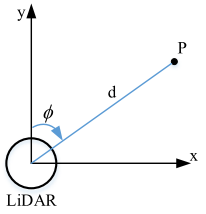

FIGURE 2. LiDAR output.

Assume that the LiDAR output s consists of the true value $\tilde{s}$ and the measurement noise $v_s \in \mathbf{R}^2$. Let δd and $\delta\phi$ be the measurement noises of distance and heading angle, respectively. We can model the LiDAR measurement output as follows:

$$s = \tilde{s} + v_s \tag{1}$$

or

$$\begin{bmatrix} x_s \\ y_s \end{bmatrix} = \begin{bmatrix} d\sin\phi \\ d\cos\phi \end{bmatrix} = \begin{bmatrix} (\tilde{d}+\delta_d)\sin(\tilde{\phi}+\delta_\phi) \\ (\tilde{d}+\delta_d)\cos(\tilde{\phi}+\delta_\phi) \end{bmatrix} \approx \begin{bmatrix} \tilde{x}_s \\ \tilde{y}_s \end{bmatrix} + D\begin{bmatrix} \delta_d \\ \delta_\phi \end{bmatrix} \tag{2}$$

where $D = \begin{bmatrix} \sin\phi & d\cos\phi \\ \cos\phi & -d\sin\phi \end{bmatrix}$. We assume that δ_d and δ_ϕ are independent and zero mean white Gaussian noises, where covariance are given by:

$$R_d^2 = E\{\delta_d^2\}, \quad R_\phi^2 = E\{\delta_\phi^2\}. \tag{3}$$

The covariance of LiDAR measurement noises can be computed as follows:

$$E\{v_s v_s^T\} = D\begin{bmatrix} R_d^2 & 0 \\ 0 & R_\phi^2 \end{bmatrix} D^T, \tag{4}$$

where superscript "T" denotes the transpose.

In this paper, R_ϕ is considered to be constant while R_d is assumed to depend on measured distance. An experiment is given in Section IV to find the model of R_d.

B. SINGLE LiDAR DATA PROCESSING

For each LiDAR, we manually assign the boundary of the walking area (polygon in Fig. 3). Each segment scan data is then divided into clusters which consist of leg scan data. After estimating the center point of each cluster, a simple algorithm is used to classify left and right legs center points. Except the center point estimation part, the details of other parts can be found in previous study [24]. In this paper, we propose a new human leg center point estimation algorithm which includes the measurement noises in the LiDAR output model.

Human leg center point estimation algorithm: The human leg is modeled as a circle with a fixed radius. Let $\tilde{r}_h \in \mathbf{R}$ and $\tilde{c} \in \mathbf{R}^2$ denote the true values of human leg radius and center point coordinate, respectively (see the right side of Fig. 3). The $\tilde{r}_h$ consists of the estimated value $\hat{r}_h$ which is manually measured by a tape, and a small error $r_{h,e}$. This algorithm is to estimate the error of the center point estimation c_e, then use it to correct the center point coordinate.

Assume that the leg cluster consists of n scan data points s_i. The circle fitting equation for a sample data is as follows:

$$\begin{aligned} \tilde{r}_h &= \|\tilde{s}_i - \tilde{c}\| \\ \hat{r}_h + r_{h,e} &= \|s_i - v_{s,i} - \hat{c} - c_e\| \\ &\approx \|s_i - \hat{c}\| + \frac{\partial f}{\partial c_e}c_e + \frac{\partial f}{\partial v_{s,i}}v_{s,i}, \end{aligned} \tag{5}$$

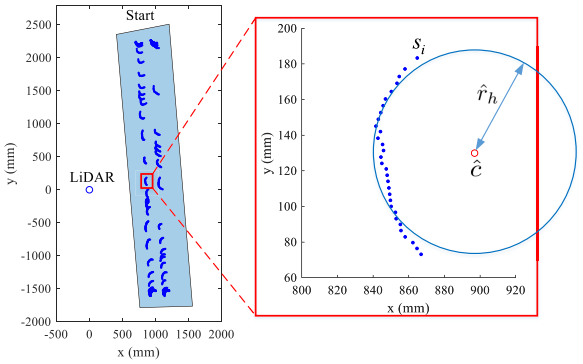

FIGURE 3. An example of walking scan data detection (blue dots in left side) and a cluster center point estimation (red circle in right side).

where $f = \|s_i - v_{s,i} - \hat{c} - c_e\|$ and $\frac{\partial f}{\partial c_e} = \frac{\partial f}{\partial v_{s,i}} = -\frac{(s_i-\hat{c})^T}{\|s_i-\hat{c}\|} = h_i(s_i, \hat{c})$. The following equation is the measurement equation for a sample scan data s_i in the cluster:

$$z_i = \hat{r}_h - \|s_i - \hat{c}\| = h_i(s_i,\hat{c})c_e + \begin{bmatrix} h_i(s_i,\hat{c}) & -1 \end{bmatrix}\begin{bmatrix} v_{s,i} \\ r_{h,e} \end{bmatrix}. \tag{6}$$

Then for a cluster, the measurement equation becomes:

$$z = Hc_e + Bw, \tag{7}$$

where $z = \begin{bmatrix} \hat{r}_h - \|s_1 - \hat{c}\| \\ \vdots \\ \hat{r}_h - \|s_n - \hat{c}\| \end{bmatrix} \in \mathbf{R}^n$, $H = \begin{bmatrix} h_1 \\ \vdots \\ h_n \end{bmatrix} \in \mathbf{R}^{n\times 2}$, $w = \begin{bmatrix} v_{s,1} \\ \vdots \\ v_{s,n} \\ r_{h,e} \end{bmatrix} \in \mathbf{R}^{2n+1}$, and $B = \begin{bmatrix} h_1 & 0 & \dots & 0 & -1 \\ 0 & h_2 & \dots & 0 & -1 \\ 0 & 0 & \dots & 0 & -1 \\ \vdots & \vdots & \vdots & \vdots & \vdots \\ 0 & 0 & \dots & h_n & -1 \end{bmatrix} \in \mathbf{R}^{n\times(2n+1)}$. The covariance matrix of measurement noises is computed as follows:

$$Q = B\mathrm{E}\{ww^T\}B^T = B\begin{bmatrix} C_1 & & & 0 \\ & C_2 & & \\ & & \ddots & \\ & & & C_n \\ 0 & & & R_{r_{h,e}} \end{bmatrix} B^T, \tag{8}$$

where $R_{r_{h,e}} = \mathrm{E}\{r_{h,e}r_{h,e}^T\}$ and $C_i (i = 1, \dots, n)$ is computed as (4).

The estimated error of the center point is then estimated as in (9):

$$\hat{c}_e = PH^T Q^{-1} z, \tag{9}$$

where $P = (H^T Q^{-1} H)^{-1}$ is the center point estimation error covariance. After that, we can update the estimated center point:

$$\hat{c}_k = \hat{c}_{k-1} + \hat{c}_e. \tag{10}$$

This process is iterated until a stop condition is satisfied: $\|\hat{c}_e\| < \gamma_c$.

The initial estimation of the leg center point is computed as follows:

$$\hat{c}_0 = \bar{c} + \frac{\bar{c}}{\|\bar{c}\|} r, \quad \text{with} \quad \bar{c} = \text{mean}\{s_i\}. \tag{11}$$

The time stamp of the estimated center point t_c is the time stamp of the middle point of the cluster.

Left/Right legs classification: After estimating the center points of human leg cluster, we will classify these center points into left and right side. Firstly, the center line formed by middle points of two center points in a scan segment is estimated. This center line divides the center points into two sides. Then, the left and right legs can be classified easily. The details of this part can be found in [24].

For each LiDAR, the center points, estimation error covariances and time stamps are now classified into left (l) and right (r) sides: $\{c_{l,L}, t_{c,l,L}, P_{l,L}\}$ and $\{c_{r,L}, t_{c,r,L}, P_{r,L}\}$, where $L = 1, 2, 3$ represents LiDARs. Due to the occlusion, which happens when the laser signal to the farther leg is stopped by the closer leg, the center points and their time stamps can be missed at some scans. In this proposed method, the missing center points are estimated using the eighth-order splines algorithm. Therefore, the time stamps of the missing center points are required.

Let $\tau_{l,L}$ and $\tau_{r,L}$ denote the full time stamps of left and right legs of LiDAR L which consists of classified time stamps and the estimated missing time stamps. We assume that the time interval between missing time stamp and the previous adjacent available time stamp equals to sampling period T_s. The equations to estimate τ are given in Algorithm 1.

Algorithm 1 Estimation of Full Time Stamps

Require: $t_{c,l(r),L}, T_s$
Ensure: $\tau_{l(r),L}$
1: $\tau_{l(r),L,1} \leftarrow t_{c,l(r),L,1}$
2: **for** $2 \le i \le N_{seg}$ **do**
3: **if** i `is missing` **then**
4: $\tau_{l(r),L,i} \leftarrow \tau_{l(r),L,i-1} + T_s$
5: **else**
6: $\tau_{l(r),L,i} \leftarrow t_{c,l(r),L,i}$
7: **end if**
8: **end for**

Finally, the outputs of the single LiDAR processing part are $\{c_{l,L}; t_{c,l,L}; \tau_{l,L}; P_{l,L}\}$ and $\{c_{r,L}; t_{c,r,L}; \tau_{r,L}; P_{r,L}\}$. Note that, these center points are expressed in the Cartesian coordinate frame.

C. CALIBRATION ALGORITHM

The data of each LiDAR are expressed on its own coordinate. To fuse these data, they need to be transformed in the same coordinate system. In this paper, we propose a calibration algorithm of multiple 2D LiDARs using a cylinder with a known radius $\hat{r}_c$. The cylinder is placed at m different positions in the LiDARs tracking range (Fig. 6 and Fig. 12). At each position, we capture one second of scan data from three LiDARs. In contrast with other methods, the center points of the cylinder at all positions and the calibration parameters are estimated at the same time in our proposed method. Also, the measurement errors of LiDAR are considered to reduce the estimation errors.

Suppose that we choose a LiDAR coordinate system as a reference coordinate (call LiDAR 1). The aim of the calibration process is to find the transformation matrix $\left[R(\tilde{\theta})\ \tilde{T}\right] \in \mathbf{R}^{2\times 3}$ between LiDAR 1 and the others, where $\theta \in \mathbf{R}$ and $T \in \mathbf{R}^2$ represent the rotation angle and translation vector, respectively.

Let x_c denote the calibration state vector that consists of the estimation of the cylinder's center points at m positions and the calibration parameters between LiDAR 1 and the others:

$$x_c = \left[c_1^T \ \dots \ c_m^T \ \theta_{12} \ T_{12}^T \ \theta_{13} \ T_{13}^T\right]^T \in \mathbf{R}^{2m+6\times 1}.$$

Let $s_{i_{L,k}}$ denote a sample measurement data of LiDAR, where $L = 1, 2, 3$ represents LiDARs, $k = 1, \dots, m$ denotes the position of cylinder, and $i_{L,k} = 1, \dots, N_{L,k}$ is the discrete index of the scan data of LiDAR L at position k of cylinder. $N_{L,k}$ is the number of cylinder scan data of LiDAR L at position k of cylinder.

1) INITIALIZATION

To estimate the initial state vector $\hat{x}_{c,0}$, the cylinder's center points at each position k (expressed in each LiDAR coordinate) ${}^L c_{L,k,0}$ are firstly estimated using least square fitting algorithm of circle:

$$\min_{{}^L c_{L,k,0}} \sum_{i_{L,k}=1}^{N_{L,k}} ((s_{i_{L,k}} - c_{L,k,0})^2 - \hat{r}_c^2)^2. \tag{12}$$

The m cylinder's center points estimated from LiDAR 1 scan data are chosen as the m initial estimated of cylinder's center points in the state vector.

Then the initial calibration parameters $(\hat{\theta}_{1L,0}, \hat{T}_{1L,0}, L = 2, 3)$ are estimated using least square method to solve the following linear model:

$${}^1 c_{1,k,0} = R(\hat{\theta}_{1L,0}) {}^L c_{L,k,0} + \hat{T}_{1L,0}. \tag{13}$$

2) THE SMALL ERRORS ESTIMATION

Due to the measurement noises in LiDAR output, the estimated calibration state vector always has errors. In this proposed algorithm, these errors are estimated and used to correct the calibration state vector.

The error state vector $x_{c,e}$ consists of the estimation errors of cylinder center points at m positions $c_{k,e} \in \mathbf{R}^2, k = 1, \dots, m$ (expressed in LiDAR 1 coordinate) and the estimation errors of rotation angles and translation vectors from LiDAR 1 to the others $(\theta_{12,e}, T_{12,e}), (\theta_{13,e}, T_{13,e})$:

$$x_{c,e} = \left[c_{1,e}^T \ \dots \ c_{m,e}^T \ \theta_{12,e} \ T_{12,e}^T \ \theta_{13,e} \ T_{13,e}^T\right]^T.$$

Since the estimated cylinder center points are expressed in LiDAR 1 coordinate, the circle fitting equations for each

LiDAR at a position k are as follows:

$$\text{LiDAR 1: } \tilde{r}_c = \|\tilde{s}_{i_{1,k}} - \tilde{c}_k\| \tag{14}$$

$$\text{LiDAR 2: } \tilde{r}_c = \|R(\tilde{\theta}_{12})\tilde{s}_{i_{2,k}} + \tilde{T}_{12} - \tilde{c}_k\| \tag{15}$$

$$\text{LiDAR 3: } \tilde{r}_c = \|R(\tilde{\theta}_{13})\tilde{s}_{i_{3,k}} + \tilde{T}_{13} - \tilde{c}_k\|. \tag{16}$$

For LiDAR 1, the measurement equation is similar to (5) and (6):

$$z_{i_{1,k}} = \hat{r}_c - \|s_{i_{1,k}} - \hat{c}_k\| = h_{i_{1,k}} c_{k,e} + \begin{bmatrix} h_{i_{1,k}} & -1 \end{bmatrix} \begin{bmatrix} v_{s_{i_{1,k}}} \\ r_{c,e} \end{bmatrix}, \tag{17}$$

with $h_{i_{1,k}} = -\frac{(s_{i_{1,k}} - \hat{c}_k)^T}{\|s_{i_{1,k}} - \hat{c}_k\|}$ and $v_{s_{i_{1,k}}} \in \mathbf{R}^2$ is the measurement errors of sample data $s_{i_{1,k}}$.

For LiDAR $L = 2, 3$, using the assumption $\tilde{\theta} = \hat{\theta} + \theta_e$, we approximate the rotation matrix as follows:

$$\begin{aligned} R(\tilde{\theta}) &= \begin{bmatrix} \cos\tilde{\theta} & -\sin\tilde{\theta} \\ \sin\tilde{\theta} & \cos\tilde{\theta} \end{bmatrix} = R(\hat{\theta})R(\theta_e) \\ &\approx R(\hat{\theta}) + G(\hat{\theta})\theta_e \end{aligned} \tag{18}$$

where $G(\hat{\theta}) = R(\hat{\theta}) \begin{bmatrix} 0 & -1 \\ 1 & 0 \end{bmatrix}$.

By inserting (18) into (15) and (16) and replacing the true value with the estimated and error values, we have:

$$\begin{aligned} \hat{r}_c + r_e &= \|[R(\hat{\theta}_{1L}) + G(\hat{\theta}_{1L})\theta_{1L,e}](s_{i_{L,k}} - v_{s_{i_{L,k}}}) + \hat{T}_{1L} \\ &\quad + T_{1L,e} - \hat{c}_k - c_{k,e}\| \\ &\approx \|R(\hat{\theta}_{1L})s_{i_{L,k}} + \hat{T}_{1L} - \hat{c}_k\| + \frac{\partial g}{\partial c_{k,e}} c_{k,e} \\ &\quad + \frac{\partial g}{\partial \theta_{1L,e}} \theta_{1L,e} + \frac{\partial g}{\partial T_{1L,e}} T_{1L,e} + \frac{\partial g}{\partial v_{s_{i_{L,k}}}} v_{s_{i_{L,k}}}, \end{aligned}$$

where $g = \|R(\hat{\theta}_{1L})s_{i_{L,k}} + \hat{T}_{1L} - \hat{c}_k - R(\hat{\theta}_{1L})v_{s_{i_{L,k}}} + G(\hat{\theta}_{1L})s_{i_{L,k}}\theta_{1L,e} + T_{1L,e} - c_{k,e}\|$.

Then the measurement equation for LiDAR $L = 2, 3$ is given as follows:

$$\begin{aligned} z_{i_{L,k}} &= \hat{r}_c - \|R(\hat{\theta}_{1L})s_{i_{L,k}} + \hat{T}_{1L} - \hat{c}_k\| \\ &= p_{i_{L,k}} c_{k,e} + q_{i_{L,k}} \theta_{1L,e} + p_{i_{L,k}} T_{1L,e} \\ &\quad + \begin{bmatrix} o_{i_{L,k}} & -1 \end{bmatrix} \begin{bmatrix} v_{s_{i_{L,k}}} \\ r_{c,e} \end{bmatrix}, \end{aligned} \tag{19}$$

where $p_{i_{L,k}} = -\frac{(R(\hat{\theta}_{1L})s_{i_{L,k}} + \hat{T}_{1L} - \hat{c}_k)^T}{\|R(\hat{\theta}_{1L})s_{i_{L,k}} + \hat{T}_{1L} - \hat{c}_k\|}$, $o_{i_{L,k}} = p_{i_{L,k}} R(\hat{\theta}_{1L})$, and $q_{i_{L,k}} = -p_{i_{L,k}} G(\hat{\theta}_{1L}) s_{i_{L,k}}$.

The measurement equation for all m positions of cylinder is as follows:

$$z_c = H_c x_{c,e} + B_c w_c, \tag{20}$$

where

$$z_c = \begin{bmatrix} \hat{r}_c - \|s_{i_{1,1}} - \hat{c}_1\| \\ \hat{r}_c - \|R(\hat{\theta}_{12})s_{i_{2,1}} + \hat{T}_{12} - \hat{c}_1\| \\ \hat{r}_c - \|R(\hat{\theta}_{13})s_{i_{3,1}} + \hat{T}_{13} - \hat{c}_1\| \\ \hat{r}_c - \|s_{i_{1,2}} - \hat{c}_2\| \\ \hat{r}_c - \|R(\hat{\theta}_{12})s_{i_{2,2}} + \hat{T}_{12} - \hat{c}_2\| \\ \hat{r}_c - \|R(\hat{\theta}_{13})s_{i_{3,2}} + \hat{T}_{13} - \hat{c}_2\| \\ \vdots \\ \hat{r}_c - \|s_{i_{1,m}} - \hat{c}_m\| \\ \hat{r}_c - \|R(\hat{\theta}_{12})s_{i_{2,m}} + \hat{T}_{12} - \hat{c}_m\| \\ \hat{r}_c - \|R(\hat{\theta}_{13})s_{i_{3,m}} + \hat{T}_{13} - \hat{c}_m\| \end{bmatrix}, w_c = \begin{bmatrix} v_{s_{i_{1,1}}} \\ v_{s_{i_{2,1}}} \\ v_{s_{i_{3,1}}} \\ v_{s_{i_{1,2}}} \\ v_{s_{i_{2,2}}} \\ v_{s_{i_{3,2}}} \\ \vdots \\ v_{s_{i_{1,m}}} \\ v_{s_{i_{2,m}}} \\ v_{s_{i_{3,m}}} \\ r_{c,e} \end{bmatrix}, z_c \in \mathbf{R}^{N_a}, w_c \in \mathbf{R}^{2N_a+1}, H_c \in \mathbf{R}^{N_a \times 2m+6} \text{ and } B_c \in \mathbf{R}^{N_a \times 2N_a+1},$$

with $N_a = \sum_{L=1}^{3} \sum_{k=1}^{m} N_{L,k}$.

The computation of covariance matrix of measurement noise Q_c is similar to (8):

$$Q_c = B_c \mathrm{E}\{w_c w_c^T\} B_c^T. \tag{21}$$

Similarly to (9) and (10), we can estimate the error state vector and update the calibration state vector as follows:

$$\hat{x}_{c,e} = (H_c^T Q_c^{-1} H_c)^{-1} H_c^T Q_c^{-1} z_c \tag{22}$$

$$\hat{x}_{c,j} = \hat{x}_{c,j-1} + \hat{x}_{c,e}. \tag{23}$$

A stop condition is also used to stop the iteration: $\|\hat{x}_{c,e}\| < \gamma_c$. The final $\hat{x}_c$ is the estimation result of cylinder's center points and the calibration parameters $(\tilde{\theta}_{12}, \tilde{T}_{12})$, $(\tilde{\theta}_{13}, \tilde{T}_{13})$.

D. DATA COMBINATION

Using the estimated calibration parameters, we transform the estimated human left/right legs center points and their estimation error covariances from LiDAR 2 and 3 into LiDAR 1 (reference) coordinate system as follows:

$${}^1c_{l(r),L} = R(\tilde{\theta}_{1L})^L c_{l(r),L} + \tilde{T}_{1L}, \tag{24}$$

$${}^1P_{l(r),L} = R^T(\tilde{\theta}_{1L})^L P_{l(r),L} R(\tilde{\theta}_{1L}) \quad L = 2, 3. \tag{25}$$

Then the transformed human leg center points from three LiDARs are combined for each left and right side. Let $S_{l(r)} = \{c_{l(r)}, t_{c,l(r)}, \tau_{l(r)}, P_{l(r)}\}$ denote the combination of three LiDARs for the left (right) side, where $c_{l(r)} = \begin{bmatrix} {}^1c_{l(r),1} & {}^1c_{l(r),2} & {}^1c_{l(r),3} \end{bmatrix}$, $t_{l(r)} = \begin{bmatrix} t_{c,l(r),1} & t_{c,l(r),2} & t_{c,l(r),3} \end{bmatrix}$, $\tau_{l(r)} = \begin{bmatrix} \tau_{l(r),1} & \tau_{l(r),2} & \tau_{l(r),3} \end{bmatrix}$, and $P_{l(r)} = \begin{bmatrix} {}^1P_{l(r),1} & {}^1P_{l(r),2} & {}^1P_{l(r),3} \end{bmatrix}$.

The combination data are then sorted in ascending order of time. The sorted data are denoted as $S^*_{l(r)} = \{c^*_{l(r)}, t^*_{c,l(r)}, \tau^*_{l(r)}, P^*_{l(r)}\}$.

As explained in single LiDAR processing, the occlusion between legs can result the missing center points in $c_{l(r)}$. This leads the discontinuity in the trajectory of the leg. To solve this problem, an eighth-order splines algorithm is used to interpolate and smooth the center points data [32].

E. QUADRATIC OPTIMIZATION-BASED EIGHTH-ORDER SPLINES ALGORITHM

In this section, the splines function of human leg center points $\zeta_{l(r)}$ are derived using the data set $S^*_{l(r)}$. For simplicity, we remove the subscript $l(r)$ in the following equations.

Given the center points data set $c^*_i = f(t^*_{c,i}), i \in [0, N]$, the i-th spline segment of ζ is given by:

$$\begin{aligned}\zeta(t) &= \zeta_i(t), \quad t \in [t^*_{c,i-1}, t^*_{c,i}], \quad (i = 1, \ldots, N)\\ \zeta_i(t) &= \psi_i(t - t^*_{c,i-1})\\ \psi_i(t) &= \sum_{k=0}^{7} a_{i,k} t^k, \quad t \in [0, \bar{T}], \quad i = 1, \ldots, N \end{aligned} \tag{26}$$

where $\bar{T}$ is the normalized length of each spline segment and $a_{i,k} \in \mathbf{R}^{2\times 1}$ are the coefficients of the i-th spline segment.

The requirement of continuity of $\zeta(t)$ and its first three derivatives at the $(N-1)$ interior knots results in the following equation:

$$\begin{bmatrix} \zeta_{i-1} \\ \zeta'_{i-1} \\ \zeta''_{i-1} \\ \zeta'''_{i-1} \\ \zeta_i \\ \zeta'_i \\ \zeta''_i \\ \zeta'''_i \end{bmatrix} = A \begin{bmatrix} a_{i,0} \\ a_{i,1} \\ a_{i,2} \\ a_{i,3} \\ a_{i,4} \\ a_{i,5} \\ a_{i,6} \\ a_{i,7} \end{bmatrix}, \quad i = 1, \ldots, N \tag{27}$$

where $A \in \mathbf{R}^{16\times 16}$ and is given in (28). I_2 and O_2 represent the 2×2 identity and zeros matrices, respectively.

Defining $\bar{u}(\bar{T}) = \begin{bmatrix} I_2 & \bar{T}I_2 & \bar{T}^2 I_2 & \bar{T}^3 I_2 & \bar{T}^4 I_2 & \bar{T}^5 I_2 & \bar{T}^6 I_2 & \bar{T}^7 I_2 \end{bmatrix}$ and $\bar{a}_i = \begin{bmatrix} a^T_{i,0} & a^T_{i,1} & a^T_{i,2} & a^T_{i,3} & a^T_{i,4} & a^T_{i,5} & a^T_{i,6} & a^T_{i,7} \end{bmatrix}^T$, we have:

$$\begin{aligned}\zeta'_i &= \bar{u}(\bar{T}) D_1 \bar{a}_i\\ \zeta''_i &= \bar{u}(\bar{T}) D_1^2 \bar{a}_i\\ \zeta'''_i &= \bar{u}(\bar{T}) D_1^3 \bar{a}_i, \end{aligned} \tag{29}$$

where $D_1 = \begin{bmatrix} O_2 & I_2 & O_2 & O_2 & O_2 & O_2 & O_2 & O_2 \\ O_2 & O_2 & 2I_2 & O_2 & O_2 & O_2 & O_2 & O_2 \\ O_2 & O_2 & O_2 & 3I_2 & O_2 & O_2 & O_2 & O_2 \\ O_2 & O_2 & O_2 & O_2 & 4I_2 & O_2 & O_2 & O_2 \\ O_2 & O_2 & O_2 & O_2 & O_2 & 5I_2 & O_2 & O_2 \\ O_2 & O_2 & O_2 & O_2 & O_2 & O_2 & 6I_2 & O_2 \\ O_2 & O_2 & O_2 & O_2 & O_2 & O_2 & O_2 & 7I_2 \\ O_2 & O_2 & O_2 & O_2 & O_2 & O_2 & O_2 & O_2 \end{bmatrix}$.

Among all piecewise continuous polynomials that satisfy the above criteria, find the one that minimizes the function:

$$\begin{aligned} J = &\sum_{i=0}^{N} (\zeta_i - c^*_i)^T P^{*-1}_i (\zeta_i - c^*_i)\\ &+ \sum_{k=1}^{N} \int_0^{\bar{T}} \left\{ \frac{\bar{T}}{h_k} \alpha_1 \left(\zeta'_k(t)\right)^T \zeta'_k(t) + \frac{\bar{T}^3}{h_k^3} \alpha_2 \left(\zeta''_k(t)\right)^T \zeta''_k(t) \right.\\ &\left. + \frac{\bar{T}^5}{h_k^5} \alpha_3 \left(\zeta'''_k(t)\right)^T \zeta'''_k(t) \right\} dt, \end{aligned} \tag{30}$$

where $\zeta_i \equiv \zeta(t^*_{c,i})$, $h_k = t^*_{c,k} - t^*_{c,k-1}$ is the knot spacing, and P^*_i is the estimation error covariance of c^*_i. The parameter $\alpha_j (j = 1, 2, 3)$ is to control the magnitude of each of the derivatives of the spline.

If we use $\bar{T} = 1$ as the normalized spline segment length, the cost function (30) becomes:

$$\begin{aligned} J = &\sum_{i=0}^{N} (\zeta_i - c^*_i)^T P^{*-1}_i (\zeta_i - c^*_i)\\ &\times \sum_{k=1}^{N} \int_0^{1} \left\{ \frac{\alpha_1}{h_k} \left(\zeta'_k(t)\right)^T \zeta'_k(t) + \frac{\alpha_2}{h_k^3} \left(\zeta''_k(t)\right)^T \zeta''_k(t) \right.\\ &\left. + \frac{\alpha_3}{h_k^5} \left(\zeta'''_k(t)\right)^T \zeta'''_k(t) \right\} dt. \end{aligned} \tag{31}$$

The integration of three derivatives can be computed using (29) as follows:

$$\begin{aligned} \int_0^1 \left(\zeta'_k(t)\right)^T \zeta'_k(t) dt &= \bar{a}_k^T D_1^T \int_0^1 \left(\bar{u}^T(t)\bar{u}(t)\right) dt D_1 \bar{a}_k\\ &= \bar{a}_k^T D_1^T Q D_1 \bar{a}_k = \bar{a}_k^T B \bar{a}_k\\ \int_0^1 \left(\zeta''_k(t)\right)^T \zeta''_k(t) dt &= \bar{a}_k^T (D_1^2)^T Q (D_1^2) \bar{a}_k = \bar{a}_k^T C \bar{a}_k\\ \int_0^1 \left(\zeta'''_k(t)\right)^T \zeta'''_k(t) dt &= \bar{a}_k^T (D_1^3)^T Q (D_1^3) \bar{a}_k = \bar{a}_k^T D \bar{a}_k, \end{aligned} \tag{32}$$

where

$$Q = \int_0^1 \left(\bar{u}^T(t)\bar{u}(t)\right) dt$$

$$A = \begin{bmatrix} I_2 & O_2 & O_2 & O_2 & O_2 & O_2 & O_2 & O_2 \\ O_2 & I_2 & O_2 & O_2 & O_2 & O_2 & O_2 & O_2 \\ O_2 & O_2 & 2I_2 & O_2 & O_2 & O_2 & O_2 & O_2 \\ O_2 & O_2 & O_2 & 6I_2 & O_2 & O_2 & O_2 & O_2 \\ I_2 & \bar{T}I_2 & \bar{T}^2 I_2 & \bar{T}^3 I_2 & \bar{T}^4 I_2 & \bar{T}^5 I_2 & \bar{T}^6 I_2 & \bar{T}^7 I_2 \\ O_2 & I_2 & 2\bar{T}I_2 & 3\bar{T}^2 I_2 & 4\bar{T}^3 I_2 & 5\bar{T}^4 I_2 & 6\bar{T}^5 I_2 & 7\bar{T}^6 I_2 \\ O_2 & O_2 & 2I_2 & 6\bar{T}I_2 & 12\bar{T}^2 I_2 & 20\bar{T}^3 I_2 & 30\bar{T}^4 I_2 & 42\bar{T}^5 I_2 \\ O_2 & O_2 & O_2 & 6I_2 & 24\bar{T}I_2 & 60\bar{T}^2 I_2 & 120\bar{T}^3 I_2 & 210\bar{T}^4 I_2 \end{bmatrix} \tag{28}$$

$$= \begin{bmatrix} I_2 & \frac{1}{2}I_2 & \frac{1}{3}I_2 & \frac{1}{4}I_2 & \frac{1}{5}I_2 & \frac{1}{6}I_2 & \frac{1}{7}I_2 & \frac{1}{8}I_2 \\ \frac{1}{2}I_2 & \frac{1}{3}I_2 & \frac{1}{4}I_2 & \frac{1}{5}I_2 & \frac{1}{6}I_2 & \frac{1}{7}I_2 & \frac{1}{8}I_2 & \frac{1}{9}I_2 \\ \frac{1}{3}I_2 & \frac{1}{4}I_2 & \frac{1}{5}I_2 & \frac{1}{6}I_2 & \frac{1}{7}I_2 & \frac{1}{8}I_2 & \frac{1}{9}I_2 & \frac{1}{10}I_2 \\ \frac{1}{4}I_2 & \frac{1}{5}I_2 & \frac{1}{6}I_2 & \frac{1}{7}I_2 & \frac{1}{8}I_2 & \frac{1}{9}I_2 & \frac{1}{10}I_2 & \frac{1}{11}I_2 \\ \frac{1}{5}I_2 & \frac{1}{6}I_2 & \frac{1}{7}I_2 & \frac{1}{8}I_2 & \frac{1}{9}I_2 & \frac{1}{10}I_2 & \frac{1}{11}I_2 & \frac{1}{12}I_2 \\ \frac{1}{6}I_2 & \frac{1}{7}I_2 & \frac{1}{8}I_2 & \frac{1}{9}I_2 & \frac{1}{10}I_2 & \frac{1}{11}I_2 & \frac{1}{12}I_2 & \frac{1}{13}I_2 \\ \frac{1}{7}I_2 & \frac{1}{8}I_2 & \frac{1}{9}I_2 & \frac{1}{10}I_2 & \frac{1}{11}I_2 & \frac{1}{12}I_2 & \frac{1}{13}I_2 & \frac{1}{14}I_2 \\ \frac{1}{8}I_2 & \frac{1}{9}I_2 & \frac{1}{10}I_2 & \frac{1}{11}I_2 & \frac{1}{12}I_2 & \frac{1}{13}I_2 & \frac{1}{14}I_2 & \frac{1}{15}I_2 \end{bmatrix}.$$

Inserting (32) into (31), we have the following:

$$J = \sum_{i=0}^{N}(\zeta_i - c_i^*)^T P_i^{*-1}(\zeta_i - c_i^*) + \sum_{k=1}^{N}\left\{\frac{\alpha_1}{h_k}\left(\bar{a}_k^T B \bar{a}_k\right) + \frac{\alpha_2}{h_k^3}\left(\bar{a}_k^T C \bar{a}_k\right) + \frac{\alpha_3}{h_k^5}\left(\bar{a}_k^T D \bar{a}_k\right)\right\}. \quad (33)$$

From (27), we have

$$\bar{a}_k = A^{-1}\begin{bmatrix}\bar{\zeta}_{k-1} \\ \bar{\zeta}_k\end{bmatrix}, k = 1, \ldots, N, \quad (34)$$

where $\bar{\zeta}_i = \begin{bmatrix}\zeta_i \\ \zeta_i' \\ \zeta_i'' \\ \zeta_i'''\end{bmatrix} \in \mathbf{R}^{8\times 1}, i = 0, \ldots, N$. Let E be the matrix that satisfies $E\bar{\zeta}_i = \zeta_i$: $E = \begin{bmatrix} I_2 & O_2 & O_2 & O_2 \end{bmatrix}$. The cost function (33) becomes

$$\begin{aligned} J = &\sum_{i=0}^{N}(E\bar{\zeta}_i - c_i^*)^T P_i^{*-1}(E\bar{\zeta}_i - c_i^*) \\ &+ \sum_{k=1}^{N}\left\{\frac{\alpha_1}{h_k}\begin{bmatrix}\bar{\zeta}_{k-1}^T & \bar{\zeta}_k^T\end{bmatrix}(A^{-1})^T B A^{-1}\begin{bmatrix}\bar{\zeta}_{k-1} \\ \bar{\zeta}_k\end{bmatrix}\right. \\ &+ \frac{\alpha_2}{h_k^3}\begin{bmatrix}\bar{\zeta}_{k-1}^T & \bar{\zeta}_k^T\end{bmatrix}(A^{-1})^T C A^{-1}\begin{bmatrix}\bar{\zeta}_{k-1} \\ \bar{\zeta}_k\end{bmatrix} \\ &\left.+ \frac{\alpha_3}{h_k^5}\begin{bmatrix}\bar{\zeta}_{k-1}^T & \bar{\zeta}_k^T\end{bmatrix}(A^{-1})^T D A^{-1}\begin{bmatrix}\bar{\zeta}_{k-1} \\ \bar{\zeta}_k\end{bmatrix}\right\}. \end{aligned} \quad (35)$$

Let U, V, and W be defined by

$$\begin{aligned} U &= (A^{-1})^T B A^{-1} = \begin{bmatrix}U_1 & U_2 \\ U_3 & U_4\end{bmatrix}, \\ V &= (A^{-1})^T C A^{-1} = \begin{bmatrix}V_1 & V_2 \\ V_3 & V_4\end{bmatrix}, \\ W &= (A^{-1})^T D A^{-1} = \begin{bmatrix}W_1 & W_2 \\ W_3 & W_4\end{bmatrix} \end{aligned}$$

where $U_k, V_k, W_k (k = 1, 2, 3, 4) \in \mathbf{R}^{8\times 8}$. Then the cost function can be rewritten as follows:

$$\begin{aligned} J &= \sum_{i=0}^{N}(E\bar{\zeta}_i - c_i^*)^T P_i^{*-1}(E\bar{\zeta}_i - c_i^*) \\ &+ \sum_{k=1}^{N}\left\{\frac{\alpha_1}{h_k}\left((\bar{\zeta}_{k-1}^T U_1 + \bar{\zeta}_k^T U_3)\bar{\zeta}_{k-1} + (\bar{\zeta}_{k-1}^T U_2 + \bar{\zeta}_k^T U_4)\bar{\zeta}_k\right)\right. \\ &+ \frac{\alpha_2}{h_k^3}\left((\bar{\zeta}_{k-1}^T V_1 + \bar{\zeta}_k^T V_3)\bar{\zeta}_{k-1} + (\bar{\zeta}_{k-1}^T V_2 + \bar{\zeta}_k^T V_4)\bar{\zeta}_k\right) \\ &\left.+ \frac{\alpha_3}{h_k^5}\left((\bar{\zeta}_{k-1}^T W_1 + \bar{\zeta}_k^T W_3)\bar{\zeta}_{k-1} + (\bar{\zeta}_{k-1}^T W_2 + \bar{\zeta}_k^T W_4)\bar{\zeta}_k\right)\right\}. \end{aligned} \quad (36)$$

Let an optimization variable $\bar{X}$ be defined by

$$\bar{X} = \begin{bmatrix}\bar{\zeta}_0 \\ \bar{\zeta}_1 \\ \cdots \\ \bar{\zeta}_N\end{bmatrix} \in \mathbf{R}^{8(N+1)\times 1}. \quad (37)$$

It is not difficult to see that (36) is a quadratic function of $\bar{X}$:

$$J(\bar{X}) = \frac{1}{2}\bar{X}^T M_1 \bar{X} + M_2 \bar{X} + M_3, \quad (38)$$

where M_1, M_2, and M_3 can be computed from (36). The M_1 and M_2 matrices are given in Appendix (M_3 matrix is omitted, since it is irrelevant in the optimization). The minimizing solution of (38) can be found by solving the following equation:

$$M_1 \bar{X}^* + M_2 = 0, \quad (39)$$

where $\bar{X}^*$ is the minimizing solution. Once these optimal values are obtained, they can be used in (34) to obtain the optimal spline coefficients $\bar{a}_k (k = 1, \ldots, N)$. After that we can estimate the spline leg center points trajectory and its velocity (first derivative) with the full time stamp τ^* using (26) and (29).

IV. EXPERIMENTAL RESULTS

A. DEPENDENCE OF MEASUREMENT ON RANGE

Since the accuracy of the RPLIDAR, which is used in this paper, is not listed in the data sheet, we did a simple experiment to investigate the relationship between R_d and the measured range. This experiment was introduced in [33]. We placed a white sheet board at different distances $D = 1$m, 2m, 3m, 4m and 5m to the LiDAR core. At each distance, the data were captured in about 10 minutes. Fig. 4a shows the experiment setup and Fig. 4b shows the scan data at each distance. We can see that the farther distance, the larger measurement errors.

The results of mean distance $\bar{D}$ and standard deviation R_d are given in Table 1.

TABLE 1. The results of mean distance $\bar{D}$ and standard deviation R_d in mm.

D	992	1984	3012	4007	5030
R_d	0.92	1.54	1.58	4.2	6.0

By fitting all the computed data, we can find the following relationship between the LiDAR range measurement standard deviation and the measured distance: $R_d = 0.001D$. In this paper, we use $R_\phi = 0.001^o$.

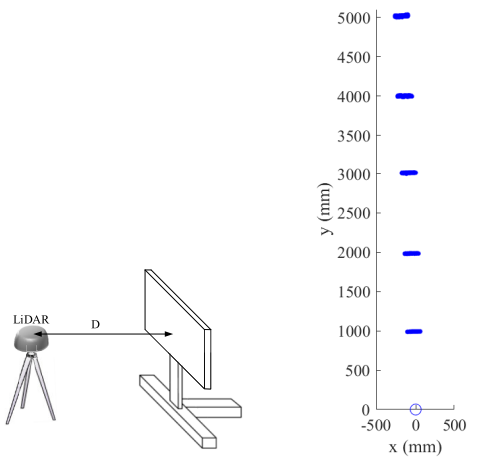

(a) Experiment setup (b) Measurement data at variable ranges (blue dots)

FIGURE 4. Dependence of measurement on range experiment.

B. HUMAN GAIT TRACKING PERFORMANCE

The proposed human gait tracking method was verified with two experiments and two male healthy subjects. The information of two subjects are given in Table 2. The parameters used in this paper are given in Table 3. Two configurations of three LiDARs system are tested: triangle and line configuration. In the first experiment, to provide the ground truth of legs trajectories we used an optical motion capture system of OptiTrack, composed of six Flex 13 cameras with a resolution of 1280 × 1024 at 120 Hz. The system can track passive spherical markers with a sub millimeter accuracy.

TABLE 2. Subjects information.

Subject	Age	Height (cm)	Weight (kg)
1	32	168	65
2	27	169	70

TABLE 3. Parameters used in this paper.

Parameters	Values	Related Equations
γ_c	0.0001	Stop threshold of (9) and (22)
$R_{r_{h,e}}$	0.01	(8)
$R_{r_{c,e}}$	0.01	(20)
$\alpha_1, \alpha_2, \alpha_3$	0.0001	(30)

1) TRIANGLE CONFIGURATION EXPERIMENT

The first experiment used the triangle configuration of three LiDARs as in Fig. 6. Each LiDAR can cover all the walking path. This configuration can minimize the occlusion between legs during walking, so that we can get more data of human leg. In this experiment, each subject walks straight 6 steps in 15 times which is divided into three speed levels: slow, normal, and fast. Two optical markers were attached to the frontside of human shanks to get the true step length estimation. Fig. 5 shows the average speed of each walking of two subjects that is computed from the optical data.

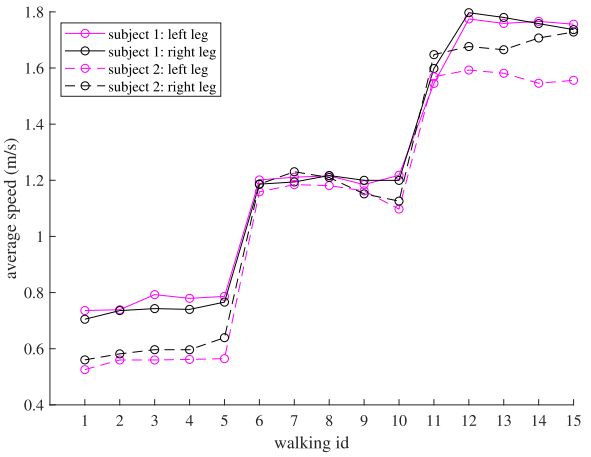

FIGURE 5. The average velocity in each walking of two subjects from OptiTrack camera system in the triangle configuration experiment.

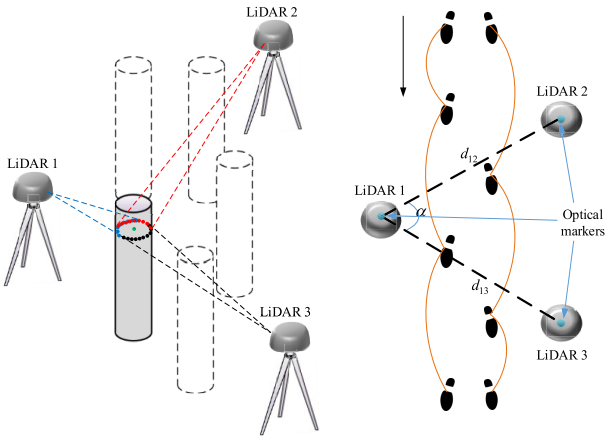

FIGURE 6. Triangle configuration of three LiDARs.

To calibrate the three LiDARs system, the cylinder is placed at 5 different positions in this experiment. The calibration parameters between three LiDARs are estimated by using the proposed calibration algorithm.

The initial estimations of calibration parameters which are estimated using (12) and (13) are considered as the results of conventional method. Using the estimated calibration parameters, we transform the measurement data into the LiDAR 1 reference coordinate system. Fig. 7 shows the results of the conventional method and the proposed method. The LiDARs positions are represented by the circles and their measurement data are represented by dots. Blue, red and black colors denote the LiDAR 1, 2 and 3, respectively. We can see that the transformation using calibration parameters of the proposed method has better performance than the conventional method.

By attaching an optical marker on the top of each LiDAR, we can estimate the true position of each LiDAR in the camera system. However, we cannot know the true heading angle of each LiDAR. Therefore, we compute the relative information of distances d_{12}, d_{13} and the angle α formed by these lines (right side of Fig. 6). The errors of these relative information compared with the camera system are given

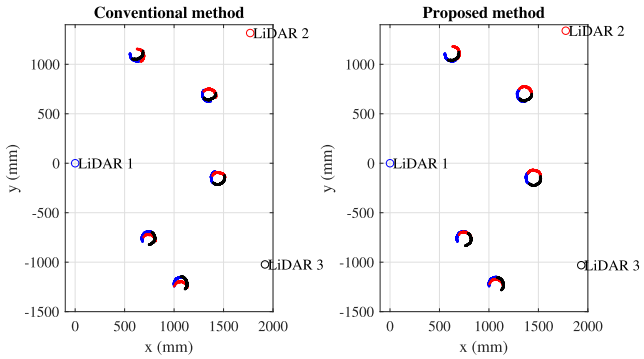

FIGURE 7. Calibration results of triangle configuration. Each LiDAR and its measurements are represented by different colors.

TABLE 4. The errors of proposed method and conventional method compared with optical camera system.

	d_{12} (mm)	d_{13} (mm)	α (degree)
Proposed method	3	2	0.000
Conventional method	17	14	0.006

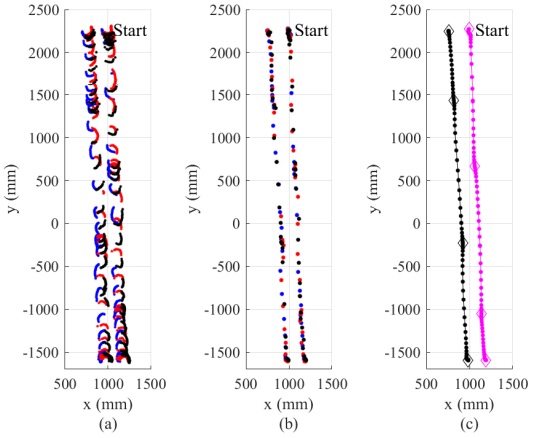

FIGURE 8. Triangle configuration results. (a): Legs scan data combination from three LiDARs. (b): Legs center points estimation. Blue, red and black colors represent data from LiDAR 1, 2 and 3 respectively. (c): Spline center points estimation and left/right leg classification. The diamond symbols represent the foot ground contact points.

in Table 4. The relative distance errors were significantly reduced using the proposed method.

The calibration parameters are then used in the human gait tracking algorithm. Fig. 8a and Fig. 8b show the combined legs scan data and their center points estimation from three LiDARs after transforming to LiDAR 1 coordinate, respectively. Fig. 9 plots three center points estimation of left leg from three LiDARs and their corresponding estimation error covariance ellipses. The distances from center points to the LiDARs are also calculated. We can see that when the distance increases, the error ellipse is also bigger. This estimation error covariance is used as an adaptive weight in the spline algorithm (P_i^* in (36)). This means a bigger weight is given on the closer center point, and vice versa.

Based on the assumption that the leg velocity is minimized when the foot is totally on the ground, we can apply a simple

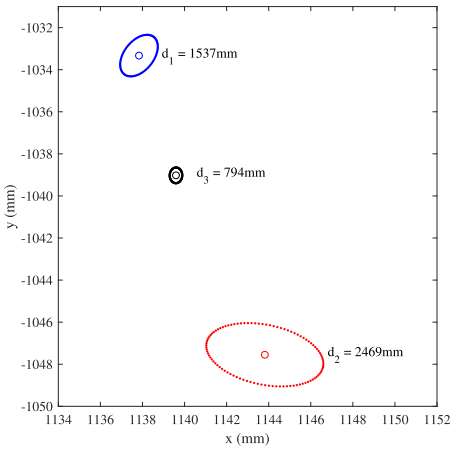

FIGURE 9. The center points estimation error covariance ellipses and their corresponding distances to the LiDAR.

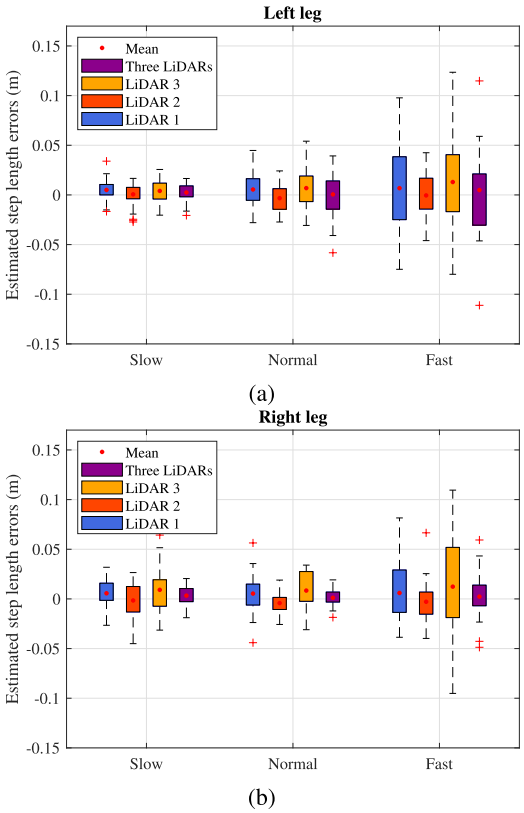

FIGURE 10. The errors of step length estimation of single LiDAR and three LiDARs systems.

threshold-based method to the estimated spline velocity to detect the walking step as in [24]. Fig. 8c shows the estimated spline trajectories of leg center points (dots) and the detected walking step (diamonds). The left and right legs are classified and represented by black and magenta dots, respectively.

We compare the estimation results from the single LiDAR system and the multiple three LiDARs system with the optical camera system. The total walking steps of two subjects are 90 for each left or right side. Fig. 10 shows the step length estimation errors of left and right legs. We can see the mean

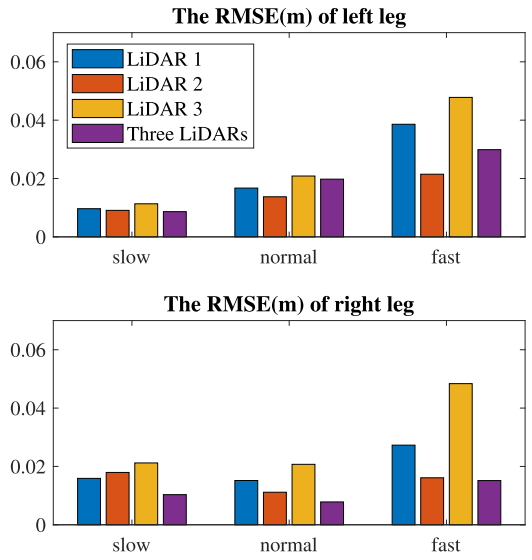

FIGURE 11. The RMSE (m) of the step length estimation from single LiDAR and three LiDARs systems.

and the maximum of the step length estimation errors of multiple LiDARs system are smaller than a single LiDAR system. After removing the outliers, the root mean square errors (RMSEs) of the step length estimation for each speed levels are given in Fig. 11. As we can see, the RMSEs increase when the walking speed increase for both single and multiple systems. The multiple LiDARs system has equal or better results compared with a single LiDAR system. As the walking speed increases, the leg scan segment data decreases that downgrades the accuracy of walking step length estimation. For the slow and normal walking speeds, the maximum RMSEs are about 0.01 m and 0.02 m, respectively. With the fast walking speed, the maximum RMSEs of multiple LiDARs system are about 0.030m and 0.015m for left and right legs, respectively.

2) LINE CONFIGURATION EXPERIMENT

The second experiment used the line configuration of three LiDARs as in Fig. 12. Each subject was asked to walk straight from the start to the end footprints in 10 times with normal and fast speed levels. The distance between two footprints is measured by a tape and equals to 20m. In this configuration, each LiDAR covers a certain distance sequentially, so that it can maximizes the tracking range of the system. An example of the available leg scan data segments of each LiDAR is shown in Fig. 13.

In this configuration, the calibration process was repeated on two LiDARs due to the large distance between them. The cylinder was placed at different positions between LiDARs 1-2 and LiDARs 1-3. Fig. 14 shows the calibration results of this configuration. Using the estimated calibration parameters, we transformed the leg scan data from LiDAR 2 and 3 systems into LiDAR 1 system. The transformation results are plotted in Fig. 15a. Fig. 15b shows the estimation results of the legs center points. We can see the occlusion between

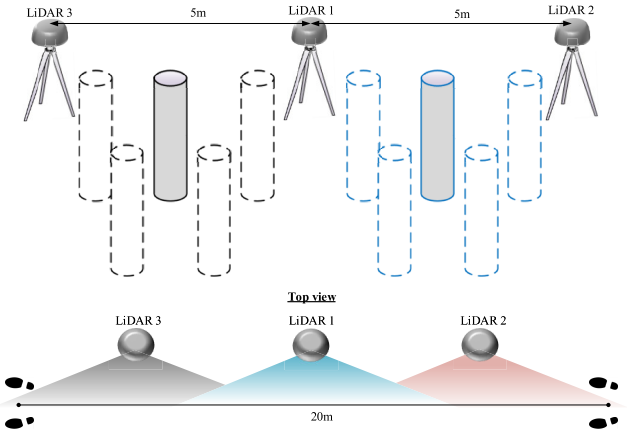

FIGURE 12. Line configuration of three LiDARs.

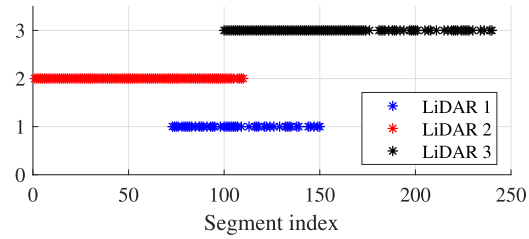

FIGURE 13. An example of the available segment indexes of each LiDAR.

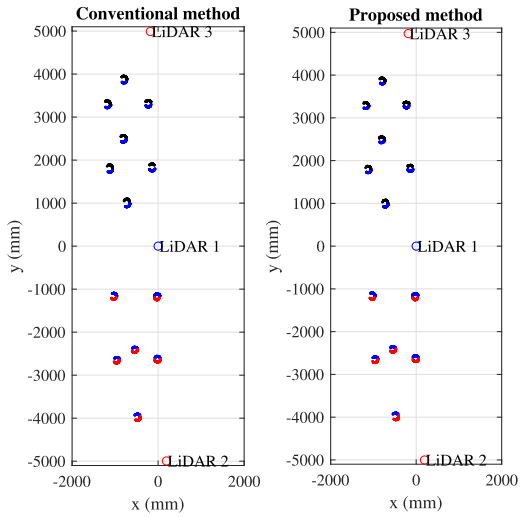

FIGURE 14. Calibration results of line configuration. Each LiDAR and its measurements are represented by a color.

legs during walking since all the LiDARs are on one side of walking path. The estimated spline trajectories of left and right legs are plotted in Fig. 15c.

Table 5 shows the estimated results of total walking distance. The estimated walking distances have maximum errors of 0.155m (0.78%) and maximum RMSE of 0.106m.

Through experimental results, our proposed method can estimate human gait parameters from multiple 2D LiDARs. However, the walking movement is limited in a horizontal plane because the 2D LiDAR only captures the depth data in two dimensional plane. In this study, only young

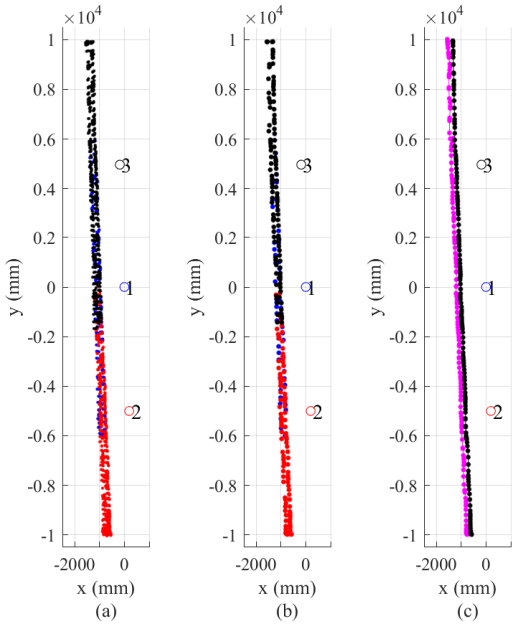

FIGURE 15. An example of line configuration results. (a): Legs scan data combination from three LiDARs. (b): Legs center points estimation. Blue, red and black colors represent data from LiDAR 1, 2 and 3 respectively. (c): Spline center points estimation and left/right leg classification.

TABLE 5. The maximum errors and RMSE of 20m walking distance estimation.

	Max (m)	Max (%)	RMSE (m)
Left leg	0.155	0.78	0.106
Right leg	0.137	0.69	0.104

and healthy people are included. The performance is better with lower walking speed which indicates that the system could also be applied for older person. However, there are many characteristics of older person that could affect to the system performance so that an experiment on the older person is necessary in the future.

V. CONCLUSION AND FUTURE WORK

In this paper, a multiple 360 degree 2D LiDAR system is used to estimate the human gait. The system is portable, low cost and can be deployed easily. With the use of multiple LiDARs, the losing data, which are caused by the occlusion between legs, is compensated and the tracking range can be increased. In the multiple sensors system, the performance critically depends on the calibration between sensors. To solve this problem, we proposed an iterative algorithm in which a cylinder with known radius is used as a specific marker. The estimation of cylinder's center points in each LiDAR coordinate system gives the optimal values of calibration parameters. After combining the data, a quadratic optimization based splines algorithm is derived to interpolate the missing data and smooth the trajectory.

The measurement noises, which are neglected in most study, are also considered in the LiDAR output. The scan data at different distance shows the effect of distance on measurement noises. Therefore, an assumption of measurement noises is given in which the standard deviation of heading angle measurement noise is a small constant value and the standard deviation of distance measurement noise is a linear function of measured distance. This measurement data model is used in the calibration process and the human leg center point estimation to enhance the accuracy.

Two configurations of three LiDARs system are given to verify the proposed method. The triangle configuration can observe the human leg scan from both side of walking path, so that it can reduce the occlusion between legs. The line configuration is to extend the tracking range of the system by arranging the LiDARs sequentially. The experimental results confirm the tracking performance of our proposed system.

By using 2D LiDARs, the computational cost is less then 3D LiDAR system that make our system possible to work in real time. This will be considered in future work. In addition, the leg scan data is currently fit by a circle with a fixed radius; however, when the leg is moving, the shape of leg scan data is usually larger. Another model of moving leg could be used to improve the system performance.

APPENDIX

The Appendix defines M_1 and M_2 matrices in (39). We use notation $M_1[i,j]$, which represents a $\mathbf{R}^{8\times 8}$ matrix extracting $8(i-1)+1 \sim 8i$ rows and $8(j-1)+1 \sim 8j$ columns of M_1. The notation of $M_2[i] \in \mathbf{R}^{1\times 8}$ is similarly defined.

$$M_1[k,k] = \begin{cases} 2(E^T {P_0^*}^{-1} E + \frac{\alpha_1}{h_1} U_1 + \frac{\alpha_2}{h_1^3} V_1 + \frac{\alpha_3}{h_1^5} W_1), \\ \text{if } k = 1 \\ \\ 2(E^T {P_{k-1}^*}^{-1} E + \frac{\alpha_1}{h_{k-1}} U_4 + \frac{\alpha_1}{h_k} U_1 \\ + \frac{\alpha_2}{h_{k-1}^3} V_4 + \frac{\alpha_2}{h_k^3} V_1 + \frac{\alpha_3}{h_{k-1}^5} W_4 + \frac{\alpha_3}{h_k^5} W_1), \\ \text{if } 2 \le k \le N \\ \\ 2(E^T {P_N^*}^{-1} E + \frac{\alpha_1}{h_N} U_4 + \frac{\alpha_2}{h_N^3} V_4 + \frac{\alpha_3}{h_N^5} W_4), \\ \text{if } k = N+1. \end{cases}$$

$$M_1[k,k+1] = 2(\frac{\alpha_1}{h_k} U_2 + \frac{\alpha_2}{h_k^3} V_2 + \frac{\alpha_3}{h_k^5} W_2), \quad k = 1,\ldots,N$$

$$M_1[k+1,k] = 2(\frac{\alpha_1}{h_k} U_3 + \frac{\alpha_2}{h_k^3} V_3 + \frac{\alpha_3}{h_k^5} W_3), \quad k = 1,\ldots,N$$

$$M_2[k] = -2(c_k^*)^T {P_{k-1}^*}^{-1} E, \quad k = 1,\ldots,N+1.$$

REFERENCES

[1] M. S. Nixon, T. Tan, and R. Chellappa, *Human Identification Based on Gait*, vol. 4. Springer, 2010.

[2] N. Khamsemanan, C. Nattee, and N. Jianwattanapaisarn, "Human identification from freestyle walks using posture-based gait feature," *IEEE Trans. Inf. Forensics Security*, vol. 13, no. 1, pp. 119–128, Jan. 2018.

[3] A. H. Snijders, B. P. van de Warrenburg, N. Giladi, and B. R. Bloem, "Neurological gait disorders in elderly people: Clinical approach and classification," *Lancet Neurol.*, vol. 6, no. 1, pp. 63–74, Jan. 2007.

[4] C. Bayón, O. Ramírez, J. I. Serrano, M. D. D. Castillo, A. Pérez-Somarriba, J. M. Belda-Lois, I. Martínez-Caballero, S. Lerma-Lara, C. Cifuentes, A. Frizera, and E. Rocon, "Development and evaluation of a novel robotic platform for gait rehabilitation in patients with cerebral palsy: CPWalker," *Robot. Auton. Syst.*, vol. 91, pp. 101–114, May 2017.

[5] A. Yorozu and M. Takahashi, "Estimation of body direction based on gait for service robot applications," *Robot. Auton. Syst.*, vol. 132, Oct. 2020, Art. no. 103603. [Online]. Available: http://www.sciencedirect.com/science/article/pii/S0921889020304437
[6] A. Mapelli, M. Zago, L. Fusini, D. Galante, A. Colombo, and C. Sforza, "Validation of a protocol for the estimation of three-dimensional body center of mass kinematics in sport," *Gait Posture*, vol. 39, no. 1, pp. 460–465, Jan. 2014.
[7] Ö. Bebek, M. A. Suster, S. Rajgopal, M. J. Fu, X. Huang, M. C. Cavusoglu, D. J. Young, M. Mehregany, A. J. van den Bogert, and C. H. Mastrangelo, "Personal navigation via high-resolution gait-corrected inertial measurement units," *IEEE Trans. Instrum. Meas.*, vol. 59, no. 11, pp. 3018–3027, Nov. 2010.
[8] P. Merriaux, Y. Dupuis, R. Boutteau, P. Vasseur, and X. Savatier, "A study of vicon system positioning performance," *Sensors*, vol. 17, no. 7, p. 1591, Jul. 2017.
[9] T. Seel, J. Raisch, and T. Schauer, "IMU-based joint angle measurement for gait analysis," *Sensors*, vol. 14, no. 4, pp. 6891–6909, Apr. 2014.
[10] R. Caldas, M. Mundt, W. Potthast, F. B. de Lima Neto, and B. Markert, "A systematic review of gait analysis methods based on inertial sensors and adaptive algorithms," *Gait Posture*, vol. 57, pp. 204–210, Sep. 2017.
[11] P. Chattopadhyay, S. Sural, and J. Mukherjee, "Frontal gait recognition from incomplete sequences using RGB-D camera," *IEEE Trans. Inf. Forensics Security*, vol. 9, no. 11, pp. 1843–1856, Nov. 2014.
[12] M. Gabel, R. Gilad-Bachrach, E. Renshaw, and A. Schuster, "Full body gait analysis with kinect," in *Proc. Annu. Int. Conf. IEEE Eng. Med. Biol. Soc.*, Aug. 2012, pp. 1964–1967.
[13] C. Benedek, B. Gálai, B. Nagy, and Z. Jankó, "LiDAR-based gait analysis and activity recognition in a 4D surveillance system," *IEEE Trans. Circuits Syst. Video Technol.*, vol. 28, no. 1, pp. 101–113, Jan. 2018.
[14] H. B. Menz, M. D. Latt, A. Tiedemann, M. M. S. Kwan, and S. R. Lord, "Reliability of the gaitrite walkway system for the quantification of temporo-spatial parameters of gait in young and older people," *Gait Posture*, vol. 20, no. 1, pp. 20–25, 2004.
[15] H. Gao, B. Cheng, J. Wang, K. Li, J. Zhao, and D. Li, "Object classification using CNN-based fusion of vision and LiDAR in autonomous vehicle environment," *IEEE Trans. Ind. Informat.*, vol. 14, no. 9, pp. 4224–4231, Sep. 2018.
[16] H. Wang, B. Wang, B. Liu, X. Meng, and G. Yang, "Pedestrian recognition and tracking using 3D LiDAR for autonomous vehicle," *Robot. Auton. Syst.*, vol. 88, pp. 71–78, Feb. 2017.
[17] S. Gatesichapakorn, J. Takamatsu, and M. Ruchanurucks, "ROS based autonomous mobile robot navigation using 2D LiDAR and RGB-D camera," in *Proc. 1st Int. Symp. Instrum., Control, Artif. Intell., Robot. (ICA-SYMP)*, Jan. 2019, pp. 151–154.
[18] Y. Xu, Y. S. Shmaliy, Y. Li, X. Chen, and H. Guo, "Indoor INS/LiDAR-based robot localization with improved robustness using cascaded FIR filter," *IEEE Access*, vol. 7, pp. 34189–34197, 2019.
[19] S. D. Sierra, J. F. Molina, D. A. Gómez, M. C. Múnera, and C. A. Cifuentes, "Development of an interface for human-robot interaction on a robotic platform for gait assistance: Agora smart walker," in *Proc. IEEE Andescon*, Aug. 2018, pp. 1–7.
[20] A. Yorozu and M. Takahashi, "Estimation of body direction based on gait for service robot applications," *Robot. Auton. Syst.*, vol. 132, Oct. 2020, Art. no. 103603.
[21] S. Yoon, H.-W. Jung, H. Jung, K. Kim, S.-K. Hong, H. Roh, and B.-M. Oh, "Development and validation of 2D-LiDAR-based gait analysis instrument and algorithm," *Sensors*, vol. 21, no. 2, p. 414, Jan. 2021.
[22] T. Pallejà, M. Teixidó, M. Tresanchez, and J. Palacín, "Measuring gait using a ground laser range sensor," *Sensors*, vol. 9, no. 11, pp. 9133–9146, Nov. 2009.
[23] A. Yorozu, T. Moriguchi, and M. Takahashi, "Improved leg tracking considering gait phase and spline-based interpolation during turning motion in walk tests," *Sensors*, vol. 15, no. 9, pp. 22451–22472, Sep. 2015.
[24] H. T. Duong and Y. S. Suh, "Human gait tracking for normal people and walker users using a 2D LiDAR," *IEEE Sensors J.*, vol. 20, no. 11, pp. 6191–6199, Jun. 2020.
[25] Q. Zhang and R. Pless, "Extrinsic calibration of a camera and laser range finder (improves camera calibration)," in *Proc. IEEE/RSJ Int. Conf. Intell. Robots Syst. (IROS)*, vol. 3, Sep. 2004, pp. 2301–2306.
[26] H. Yoo, H. J. Moon, S.-H. Kim, and S.-I. Choi, "Multi-target tracking with multiple 2D range scanners," *IEEE Access*, vol. 8, pp. 99990–99998, 2020.
[27] J.-L. Blanco, F.-A. Moreno, and J. Gonzalez, "A collection of outdoor robotic datasets with centimeter-accuracy ground truth," *Auton. Robots*, vol. 27, no. 4, pp. 327–351, Nov. 2009.
[28] K. Schenk, A. Kolarow, M. Eisenbach, K. Debes, and H.-M. Gross, "Automatic calibration of a stationary network of laser range finders by matching movement trajectories," in *Proc. IEEE/RSJ Int. Conf. Intell. Robots Syst.*, Oct. 2012, pp. 431–437.
[29] D.-G. Choi, Y. Bok, J.-S. Kim, and I. S. Kweon, "Extrinsic calibration of 2-D LiDARs using two orthogonal planes," *IEEE Trans. Robot.*, vol. 32, no. 1, pp. 83–98, Feb. 2016.
[30] F. Zhu, Y. Huang, Z. Tian, and Y. Ma, "Extrinsic calibration of multiple two-dimensional laser rangefinders based on a trihedron," *Sensors*, vol. 20, no. 7, p. 1837, Mar. 2020.
[31] D. Yin, J. Liu, T. Wu, K. Liu, J. Hyyppä, and R. Chen, "Extrinsic calibration of 2D laser rangefinders using an existing cuboid-shaped corridor as the reference," *Sensors*, vol. 18, no. 12, p. 4371, Dec. 2018.
[32] D. Simon, "Data smoothing and interpolation using eighth-order algebraic splines," *IEEE Trans. Signal Process.*, vol. 52, no. 4, pp. 1136–1144, Apr. 2004.
[33] L. Kneip, F. Tache, G. Caprari, and R. Siegwart, "Characterization of the compact hokuyo URG-04LX 2D laser range scanner," in *Proc. IEEE Int. Conf. Robot. Automat.*, May 2009, pp. 1447–1454.

HUU TOAN DUONG received the B.S. degree from the School of Electrical Engineering, Hanoi University of Science and Technology, Hanoi, Vietnam, in 2013, and the M.S. and Ph.D. degrees from the Department of Electrical, Electronic and Computer Engineering, University of Ulsan, Ulsan, South Korea, in 2016 and 2020, respectively.

He is currently a Postdoctoral Researcher with the Department of Electrical, Electronic and Computer Engineering, University of Ulsan. His current research interests include human gait analysis, motion tracking, and personal navigation systems.

YOUNG SOO SUH (Member, IEEE) received the B.S. and M.S. degrees from the Department of Control and Instrumentation Engineering, Seoul National University, Seoul, South Korea, in 1990 and 1992, respectively, and the Ph.D. degree from the Department of Mathematical Engineering and Information Physics, The University of Tokyo, Tokyo, Japan, in 1997.

He is currently a Professor with the Department of Electrical Engineering, University of Ulsan, Ulsan, South Korea. His current research interests include attitude estimation and personal navigation systems.